

Numerically “exact” simulations of a quantum Carnot cycle: Analysis using thermodynamic work diagrams

Shoki Koyanagi  and Yoshitaka Tanimura ^{a)}

Department of Chemistry, Graduate School of Science, Kyoto University, Kyoto 606-8502, Japan

(Dated: Last updated: 8 July 2022)

Numerically accurate simulations of a quantum Carnot engine were conducted in a non-perturbative and non-Markovian system-bath (SB) coupling regime based on the open quantum dynamics theory. The model includes time-dependent external fields for the subsystems controlling the isothermal and isentropic processes and for the SB interactions controlling the transition between isothermal and isentropic processes. Numerical simulations were conducted using the hierarchical equations of motion (HEOM) under these fields at different cycle frequencies. The work done to the total system and the heat exchanged with the baths were rigorously evaluated, showing that the thermal efficiency approaches the Carnot limit under a quasi-static condition. By regarding quasi-static work as free energy, we compute quantum thermodynamic variables to analyze the simulation results using thermodynamic work diagrams for the first time. Analysis of these diagrams indicated that in a strong SB coupling region, the fields for the SB interaction are major sources of work, while in other regions the field for the subsystem is a source of work. We find that the maximum efficiency is achieved in the quasi-static case and is determined solely by the temperatures of the baths, regardless of the SB coupling strength, which is a numerical manifestation of Carnot’s theorem.

I. INTRODUCTION

In 1824, Sadi Carnot proposed a reversible heat engine (which was subsequently named the Carnot engine) operating between a high-temperature (hot) bath at temperature T_1 and a low-temperature (cold) bath at temperature T_2 using gas as a working medium.¹ This heat engine performs the Carnot cycle, which consists of four reversible processes: (i) isothermal expansion, (ii) isentropic expansion, (iii) isothermal compression, and (iv) isentropic compression. Here, heat Q_1 is absorbed from the hot bath, and work is produced during the isothermal expansion process; heat Q_2 is expelled to the cold bath, and some work is lost in the isothermal compression process. The isentropic processes bridge the two isothermal processes quasi-statically by lowering or raising the temperature of the system to T_2 or T_1 , respectively. The work is done while adiabatically reducing the temperature, and the net gain of heat is equal to the work done, i.e., $W = Q_1 - Q_2$. Carnot proved that (a) the thermal efficiency of this engine is the maximum that is possible, and that (b) this maximum efficiency is determined solely by the temperatures of the heat baths (Carnot’s theorem). Moreover, the relationship $Q_1/T_1 - Q_2/T_2 = 0$ is satisfied in the Carnot cycle. To elucidate the characteristic features of a Carnot cycle, a thermodynamic work diagram (the P - V diagram) was later introduced by Clapeyron.² The work done by the system is represented by the area enclosed by the curves in the P - V diagram.

In 1848, William Thomson (Lord Kelvin) established that the temperatures appearing in the above formula

should be regarded as thermodynamic (or absolute) temperatures.³ Then, in the 1850s, the foundations of the second law of thermodynamics were established by Rudolf Clausius on the basis of Carnot’s result.^{4,5} Carnot’s result was generalized by Thomson and Clausius as $\oint dQ/T = 0$, where T is the temperature of the heat source and Q is the heat reversibly transferred to the system. In 1865, Clausius introduced entropy, which is defined as $dS = dQ/T$, and he expressed the second law of thermodynamics for heat Q as $\oint dQ/T < \oint dS = 0$ in any irreversible process.⁶ Entropy is an extensive variable that characterizes the reversibility or irreversibility of thermal processes based on the Carnot cycle, and its conjugate intensive variables is temperature. The Carnot cycle was a key element in the construction of thermodynamics.

Recently, due to the advent of nanotechnology, thermodynamic investigations have been extended to the quantum regime,^{7–19} in which the work and heat to be manipulated are quantized.^{20–30} However, such studies involve fundamental difficulties because the time evolution of a main system (subsystem) is described by quantum mechanics, while the thermal effects of the system are described by macroscopic thermodynamics and statistical mechanics for the equilibrium state. For example, in an investigation of isothermal processes, we must explicitly treat the system–bath (SB) interactions to maintain the subsystem in a state of thermal equilibrium under the influence of an external force. Because the energy scale of the SB interactions is comparable to the energy of the subsystem, we must treat not only the subsystem but also the SB interactions in a quantum-mechanically consistent manner. Moreover, the quantum description of the heat bath is also significant because the subsystem and the bath are entangled (bath entanglement), particularly in the low-temperature case.^{31–34} In an adiabatic

^{a)} Author to whom correspondence should be addressed: tanimura.yoshitaka.5w@kyoto-u.jp

process, a thermodynamic system with a large number of degrees of freedom is usually assumed to be in an equilibrium state with a quasi-static change in an extensive thermodynamic variable. An isolated quantum subsystem, however, cannot reach a thermal equilibrium state of its own, and thus its temperature cannot be defined during adiabatic processes. The definitions of thermodynamic variables in a small subsystem, in particular extensive variables such as magnetization and strain, are not clear in the quantum case.

In the present paper, to clarify the relationship between quantum mechanics and statistical thermodynamics, we conduct quantum simulations of a Carnot cycle on the basis of an SB model. Although such investigations have been conducted in a framework of open quantum dynamics theories, even in strong SB coupling cases (for example, for heat transport,^{35–49} heat engines and refrigerators,^{50–70} entropy production,^{71–73} non-equilibrium works,^{18,74} and quantum information problems,^{75,76} in addition to being applied as a context for the Jarzynski equality,^{77–79} fluctuation theorems,^{80–85} and Maxwell’s demon^{86–88}), fully quantum investigations face difficulties because of the lack of a consistent thermodynamic formulation for a thermal system described by a Hamiltonian with external time-dependent perturbations.

Recently, it was shown that heat can be defined as the change in heat-bath energy.^{48,55} The key to investigating this problem is the HEOM formalism, which enables the evaluation of the internal energies of not only the subsystem, but also the bath and the SB interactions, even in low-temperature, non-Markovian, and nonperturbative conditions.^{31–34,89–91} Although previous studies were limited to the case of isothermal transitions,^{73,79} we show that, by introducing a time-dependent SB interaction, thermal transitions between isothermal and adiabatic states can also be investigated. Then, by using HEOM to calculate the change in work and bath energy applied to the entire system, the efficiency of the heat engine under an arbitrary time-dependent external field can be evaluated without assumptions.⁹²

In addition, thermodynamic variables can be treated based on the SB model in order to perform thermodynamic analysis. For this purpose, we adopt the minimal work principle for a total isolated system expressed as $W_{\text{tot}}(t) \geq \Delta F_{\text{tot}}(t)$, where $W_{\text{tot}}(t)$ is the work done by external fields and $\Delta F_{\text{tot}}(t)$ is the change of free energy, and define the “quasi-static” Helmholtz energy (qHE) as $\Delta F_{\text{tot}}(t) = W_{\text{tot}}^{\text{qst}}(t)$ with the system driven quasi-statically by external fields. Although the evaluations of $W_{\text{tot}}(t)$ is not possible within the framework of the regular open quantum dynamics theories because the bath degrees of freedom have been reduced, we can evaluate it indirectly using the hierarchical elements in the HEOM formalism. This is because, in the HEOM formalism, the higher hierarchical elements store information about the higher cumulant of the bath coordinates, as previously demonstrated.^{44,48,55,73,79} We then show that the

Kelvin-Planck statement (or heat engine statement) of the second law of thermodynamics is validated only when we introduced a time-dependent SB interaction that describes energy conservation for adiabatic transitions.⁹²

To this end, we extend the previous study to verify the Carnot’s theorem from the HEOM approach. The Carnot engine is described as a two-level subsystem (A) coupled with harmonic heat baths (B). To control the isothermal process, we consider the external field for the system (the isothermal driving field) and, to turn the hot and cold baths on and off, we introduce two time-dependent SB interactions (the adiabatic transition fields). We then investigate the thermodynamic efficiency of the Carnot cycle under various physical conditions. In addition, using the qHE formalism, a thermodynamic work diagram of external forces (such as stresses) and their conjugate variables (such as strains), similar to Clapeyron’s P - V diagram,² are introduced to analyze the work done in the system. Such an extension can be useful for analyzing experimental results in the quantum regime, where the quantized work and heat to be manipulated.^{20–29}

The remainder of this paper is organized as follows. In Sec. II, we introduce the SB Hamiltonian and the HEOM formalism. We then describe the scheme used to calculate various thermodynamic variables based on open quantum dynamics theory. In Sec. III, we explain our model of the quantum Carnot cycle and present the simulation results under the isothermal driving and adiabatic transition fields. The conjugated properties of these variables are calculated from quasi-static work by regarding it as free energy. Thermodynamic work diagrams are presented as functions of these variables. Section IV presents concluding remarks.

II. THEORY

A. Model

We consider a subsystem A coupled to two heat baths at high and low inverse temperatures $\beta_1 = 1/k_B T_1$ and $\beta_2 = 1/k_B T_2$ as the heat sources, where k_B is the Boltzmann constant. The total Hamiltonian is expressed as

$$\hat{H}_{\text{tot}}(t) = \hat{H}_A(t) + \sum_{k=1}^2 \left(\hat{H}_I^k(t) + \hat{H}_B^k \right), \quad (1)$$

where $\hat{H}_A(t)$, $\hat{H}_I^k(t)$, and \hat{H}_B^k are the Hamiltonians of the system, k th SB interaction, and k th bath, respectively. We consider a two-level system (TLS) defined as

$$\hat{H}_A(t) = -B(t)\hat{\sigma}_z + E\hat{\sigma}_x, \quad (2)$$

where $B(t)$ is the isothermal driving field (IDF), E is the off-diagonal coupling parameter, and $\hat{\sigma}_\alpha$ ($\alpha = x, y, \text{ or } z$) are Pauli matrices. In the case of a spin system, $B(t)$ corresponds to the longitudinal magnetic field and E is

the transverse electric (Stark) field. The Hamiltonian representing the k th SB interaction and the k th bath are given by⁹²

$$\hat{H}_1^k(t) = A_k(t)\hat{V}_k \sum_j c_j^k \left[\hat{b}_j^k + (\hat{b}_j^k)^\dagger \right], \quad (3)$$

and

$$\hat{H}_B^k = \sum_j \hbar\omega_j^k \left[(\hat{b}_j^k)^\dagger \hat{b}_j^k + \frac{1}{2} \right], \quad (4)$$

respectively, where \hat{V}_k is the system operator that describes the coupling to the k th bath and $A_k(t)$ is the adiabatic transition field (ATF), which is introduced to describe the operation of an adiabatic wall between the system and the k th heat bath (e.g., the insertion or removal of the adiabatic wall or attaching or detaching the quantum system to/from the bath). Here, ω_j^k , c_j^k , \hat{b}_j^k , and $(\hat{b}_j^k)^\dagger$ are the frequency, coupling strength, and annihilation and creation operators for the j th mode of the k th bath, respectively.

Due to the Bosonic nature of the baths, all bath effects on the system are determined by the k th bath correlation function, $C_k(t) \equiv \langle \hat{X}_k(t)\hat{X}_k(0) \rangle_B$, where $\hat{X}_k \equiv \sum_j c_j^k [\hat{b}_j^k + (\hat{b}_j^k)^\dagger]$ is the collective coordinate of the k th bath and $\langle \cdots \rangle_B$ represents the average taken with respect to the canonical density operator of the baths. The bath correlation function is expressed as

$$C_k(t) = \int_0^\infty d\omega \frac{J_k(\omega)}{\pi} \left[\coth\left(\frac{\beta_k \hbar \omega}{2}\right) \cos(\omega t) - i \sin(\omega t) \right], \quad (5)$$

where $J_k(\omega) \equiv \pi \sum_j (c_j^k)^2 \delta(\omega - \omega_j^k)$ is the bath spectral density. The real part of Eq. (5) is analogous to the classical correlation function of the bath and corresponds to the fluctuations, while its imaginary part corresponds to the dissipation. The fluctuation term is related to the dissipation term through the quantum version of the fluctuation–dissipation theorem. In this paper, we use the Drude spectral density function, described as

$$J_k(\omega) = \frac{\hbar\gamma_k^2\omega}{\gamma_k^2 + \omega^2}, \quad (6)$$

where γ_k is the inverse noise correlation of the k th bath.

B. Hierarchical equations of motion

In the HEOM formalism, the set of equations of motion consists of the auxiliary density operators (ADOs).^{31–34,89–92} Here, we consider the case that the bath correlation function, Eq. (5), is written as a linear combination of exponential functions, $C_k(t) = \sum_{l=0}^{K_k} \zeta_l^k e^{-\nu_l^k |t|}$, where ν_l^k and ζ_l^k are the frequency and strength for the k th bath obtained from a Padé spectral

decomposition scheme to reduce the hierarchy size.⁹³ The ADOs introduced in the HEOM are defined by $\hat{\rho}_{\vec{n}}(t)$ with a set of index $\vec{n} = (n_1^0, \dots, n_1^{K_1}, n_2^0, \dots, n_2^{K_2})$, where n_l^k represents an integer value zero and above. The zeroth ADO, $\hat{\rho}_{\vec{0}}(t)$ with $\vec{0} = (0, 0, \dots, 0)$, corresponds to the actual reduced density operator. Then the HEOM for a IDF and ATFs are expressed as⁹²

$$\begin{aligned} \frac{\partial}{\partial t} \hat{\rho}_{\vec{n}}(t) = & \left(-\frac{i}{\hbar} \hat{H}_A^\times(t) - \sum_{k=1}^2 \sum_{l=0}^{K_k} n_l^k \nu_l^k \right) \hat{\rho}_{\vec{n}}(t) \\ & - \frac{i}{\hbar} \sum_{k=1}^2 A_k(t) \sum_{l=0}^{K_k} n_l^k \hat{\Theta}_l^k \hat{\rho}_{\vec{n} - \vec{e}_l^k}(t) \\ & - \frac{i}{\hbar} \sum_{k=1}^2 A_k(t) \sum_{l=0}^{K_k} \hat{V}_k^\times \hat{\rho}_{\vec{n} + \vec{e}_l^k}(t), \end{aligned} \quad (7)$$

where \vec{e}_l^k is the (K_k+1) -dimensional unit vector, and we introduce a set of the fluctuation-dissipation operators

$$\hat{\Theta}_0^k \equiv \left(\frac{\gamma_k}{\beta_k} + \sum_{m=1}^{K_m} \frac{\zeta_m \gamma_m^2}{\beta_k} \frac{2\gamma_k}{\gamma_k^2 - \nu_m^2} \right) \hat{V}_k^\times - \frac{i\hbar\gamma_k^2}{2} \hat{V}_k^\circ \quad (8)$$

and

$$\hat{\Theta}_l^k \equiv -\frac{\zeta_l \gamma_l^2}{\beta_k} \frac{2\nu_l}{\gamma_k^2 - \nu_l^2} \hat{V}_k^\times, \quad (9)$$

where $\hat{\Theta}^\times \hat{P} = [\hat{\Theta}, \hat{P}]$ and $\hat{\Theta}^\circ \hat{P} = \{\hat{\Theta}, \hat{P}\}$ for arbitrary operators $\hat{\Theta}$ and \hat{P} , and ν_l and ζ_l are the frequency and strength.

As temporally initial conditions, we consider the factorized initial one,

$$\hat{\rho}_{\text{tot}}(0) = \hat{\rho}_A(0) \prod_{k=1}^2 \frac{e^{-\beta_k \hat{H}_B^k}}{\text{tr}_B \{ e^{-\beta_k \hat{H}_B^k} \}},$$

where $\hat{\rho}_A(t)$ is the reduced density operator of the subsystem. To obtain the bath-entangled steady-state solution, we integrate the HEOM under the periodical external fields until all of the hierarchy elements reach a steady state.

Using the zeroth member of the hierarchy $\hat{\rho}_{\vec{0}}(t)$, the non-equilibrium internal energy of the system (or the expectation value of the system energy) at time t is evaluated as

$$U_A^{\text{neq}}(t) = \text{tr}_A \left\{ \hat{H}_A(t) \hat{\rho}_{\vec{0}}(t) \right\}. \quad (10)$$

Then, the non-equilibrium internal energy of the k th SB interaction is expressed as^{48,55,73,79}

$$U_{I_k}^{\text{neq}}(t) = A_k(t) \sum_{l=0}^{K_k} \text{tr}_A \left\{ \hat{V}_k \hat{\rho}_{\vec{e}_l^k}(t) \right\}, \quad (11)$$

where \vec{e}_l is the index for the first-order hierarchical member.

Using the HEOM formalism, we can evaluate the k th bath energy as^{73,92}

$$\begin{aligned} \frac{\partial}{\partial t} U_{B_k}^{\text{neq}}(\beta_k; t) &= A_k(t) \sum_{l=0}^{K_k} \nu_l \text{tr} \{ \hat{V} \hat{\rho}_{\bar{e}_l}(t) \} \\ &+ A_k^2(t) \gamma^2 \text{tr}_A \left\{ \hat{V}^2 \hat{\rho}_{\bar{0}}(t) \right\}. \end{aligned} \quad (12)$$

Because there is no external force applied to the bath, the k th bath heat can be obtained by integrating the above equation as

$$Q_{B_k}(\beta_k; t) = \Delta U_{B_k}^{\text{neq}}(\beta_k; t) \quad (13)$$

with $\Delta U_{B_k}^{\text{neq}}(\beta_k; t) \equiv U_{B_k}^{\text{neq}}(\beta_k; t + \delta t) - U_{B_k}^{\text{neq}}(\beta_k; t)$, where δt is the time step of a thermal process.

In this study, work is defined by the change in energy from one state to another state under a time-dependent perturbation expressed as

$$W_{\text{tot}}(t) = \int_t^{t+\delta t} dt' \text{tr} \left\{ \frac{d\hat{H}_{\text{tot}}(t')}{dt'} \hat{\rho}_{\text{tot}}(t') \right\}. \quad (14)$$

Because there is no external field for the bath, we have $W_{\text{tot}}(t) = W_{A+I}(t)$, where

$$W_{A+I}(t) \equiv W_A(t) + W_{I_1}(t) + W_{I_2}(t). \quad (15)$$

Using the HEOM, each component is evaluated as

$$W_A(t) = \int_t^{t+\delta t} dt' \text{tr}_A \left\{ \frac{\partial \hat{H}_A(t')}{\partial t} \hat{\rho}_{\bar{0}}(t') \right\}, \quad (16)$$

and

$$W_{I_k}(t) = \int_t^{t+\delta t} dt' \frac{dA_k(t')}{dt'} \sum_{l=0}^{K_k} \text{tr}_A \{ \hat{V}_k \hat{\rho}_{\bar{e}_l^*}(t') \}. \quad (17)$$

By this definition, when $W_{\text{tot}}(t) > 0$, work is done from the outside to the total system and is called ‘‘positive work’’.

Using the above results, we can evaluate the k th bath energy for $A_k(t) > 0$ from

$$\begin{aligned} \frac{\partial}{\partial t} U_{B_k}^{\text{neq}}(\beta_k; t) &= \frac{\partial}{\partial t} [U_A^{\text{neq}}(t) + U_{I_k}^{\text{neq}}(t)] \\ &- \frac{\partial}{\partial t} [W_A(t) + W_{I_k}(t)] \end{aligned} \quad (18)$$

more accurately than from Eq. (12).

C. Quasi-static free energy and thermodynamics variables

By using the above definition of work with the HEOM, the efficiency of the system driven by the IDF and ATFs can be evaluated numerically and rigorously for any cycle speed. Nevertheless, we concentrate our discussion to the

quasi-static case and attempt to quantify quantum thermodynamic variables by comparing physical quantities calculated in the HEOM with thermodynamic quantities evaluated in the quasi-static Helmholtz energy (qHE), as explained below. The work for the total system satisfies the minimum work principle, expressed as^{94–96}

$$W_{\text{tot}}(\beta; t) \geq \Delta F_{\text{tot}}(\beta; t), \quad (19)$$

which corresponds to the second law of thermodynamics. For the SB model, the above inequality has been verified numerically by using the real-time HEOM for work on the left-hand side and the imaginary-time HEOM for the free energy on the right-hand side.^{33,34,97} This is due to the fact that even when \hat{H}_A and \hat{H}_I are weakly time dependent, the steady-state solution of the HEOM is represented as the reduced density operator of the total equilibrium state expressed as $\text{tr}_B \{ \exp[-\beta(\hat{H}_A + \hat{H}_I + \hat{H}_B)] \}$.^{33,34} Then, it was found that, for a quasi-static process, we have the equality expressed within the numerical accuracy as^{73,79,92}

$$\Delta F_{\text{tot}}^{\text{qst}}(\beta; t) = W_{\text{tot}}^{\text{qst}}(\beta; t). \quad (20)$$

While the above equation holds for the total system, not the reduced system, we can utilize the qHE using the HEOM formalism because, through use of the HEOM elements, we can evaluate the total work of the system. For each component, we also have $\Delta F_{\alpha}^{\text{qst}}(\beta; t) = W_{\alpha}^{\text{qst}}(\beta; t)$ for $\alpha = A, I_1, \text{ and } I_2$, where $W_{\alpha}^{\text{qst}}(\beta; t)$ is defined by Eqs. (16) and (17) using the quasi-static solution of the HEOM, which is expressed as $\hat{\rho}_{\bar{n}}^{\text{qst}}(t)$.⁹²

In the Carnot cycle, the subsystem interacts with a single bath at a time. Then, for external fields, such as a magnetic field $B(t)$ and stress $A_k(t)$, we have $\Delta F_{\text{tot}}^{\text{qst}}(\beta; t) = \Delta F_{A+I}^{\text{qst}}(\beta; t)$ for $\beta = \beta_k$ with $k = 1$ or 2 , where $\Delta F_{A+I}^{\text{qst}}(\beta_k; t) \equiv \Delta F_A^{\text{qst}}(\beta_k; t) + \Delta F_{I_k}^{\text{qst}}(\beta_k; t)$. Then we can define the conjugate variables, such as the magnetization and strain, as⁹²

$$M^{\text{qst}}(\beta_k; t) \equiv - \frac{\partial \Delta F_A^{\text{qst}}(\beta_k; t)}{\partial B(t)} \quad (21)$$

and

$$D_k^{\text{qst}}(\beta_k; t) \equiv - \frac{\partial \Delta F_{I_k}^{\text{qst}}(\beta_k; t)}{\partial A_k(t)}. \quad (22)$$

Then, we can evaluate the above variables in terms of the state described by ADOs at time t as

$$M^{\text{qst}}(\beta_k; t) = \text{tr}_A \{ \hat{\sigma}_z \hat{\rho}_{\bar{0}}(t) \}, \quad (23)$$

and

$$D_k^{\text{qst}}(\beta_k; t) = - \sum_{l=0}^{K_k} \text{tr}_A \left\{ \hat{V}_k \hat{\rho}_{\bar{e}_l^*}(t) \right\}. \quad (24)$$

The change in the quasi-static Boltzmann entropy from time t to $t + \delta t$ can also be evaluated by differentiating

the qHE with respect to the k bath inverse temperature β_k as⁷³

$$\Delta S_{A+I}^{\text{qst}}(\beta_k; t) \equiv k_B \beta_k^2 \frac{\partial \Delta F_{A+I}^{\text{qst}}(\beta_k; t)}{\partial \beta_k}, \quad (25)$$

where we consider the case that the subsystem interacts with a single bath at a time. A comparison of this definition with von Neumann entropy using the simulation results for the Carnot cycle is given in Appendix B.

Note that $M^{\text{qst}}(\beta; t)$, $D_k^{\text{qst}}(\beta; t)$ and $\Delta S_{A+I}^{\text{qst}}(\beta; t)$ are state variables at quasi-static state because they are uniquely determined by the state specified by the quasi-equilibrium distribution at t and are independent of the pathway of work. When the subsystem consists of n non-interacting spins that are independently coupled to the heat bath, the magnitudes of the above variables are proportional to n . Thus, they are extensive properties, while $B(t)$, $A_k(t)$ and β are intensive properties.

Then the quasi-static isothermal process at temperature $T_k = 1/k_B \beta_k$ is expressed as

$$d\Delta F_{A+I}^{\text{qst}}(\beta_k; t) = -\Delta S_{A+I}^{\text{qst}}(\beta_k; t)dT_k - M^{\text{qst}}(\beta_k; t)dB - D_k^{\text{qst}}(\beta_k; t)dA_k. \quad (26)$$

III. QUANTUM CARNOT CYCLE

The conventional Carnot cycle consists of a system, described by pressure [P] and volume [V], that interacts with hot and cold baths. Although isothermal processes can be easily described by changing an external perturbation $B(t)$, there are several difficulties in realizing the Carnot cycle, even theoretically, in a nanoscale quantum system. For example, to conduct a microscopic investigation of the Carnot cycle, the thermal work done in the insertion or removal of the adiabatic wall must be included, because otherwise the energy conservation law of the total system would be violated. Accordingly, since a small isolated system cannot reach thermal equilibrium by itself, an isentropic process cannot be achieved simply by turning off the heat bath. Finally, although the Carnot cycle has been commonly characterized by the P - V diagram, in a small quantum system, the definition of extensive variables is unclear. As we explained, the quasi-static Helmholtz energy can provide the necessary means to analyze simulation results of the quantum Carnot cycle obtained from the HEOM approach.

A. Case under factorized assumption

Before presenting the computational results, we will first illustrate the B - M diagram assuming that the free energy of the TLS is determined by the partition function of the isolated TLS and that it is valid under weak and Markovian SB coupling assumptions (factorized assumption). Thus, from $F_A^0(\beta; t) = -\ln \text{tr}\{\exp[-\beta \hat{H}_A(t)]\}/\beta$,

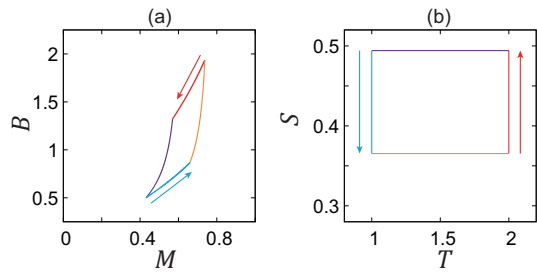


FIG. 1. (a) B - M diagram of Carnot engine driven by $B(t)$ with $B_0 = 2$ and $E = 0.5$ evaluated under the factorized assumption, i.e., $F_A(t) = -\ln \text{tr}\{\exp[-\beta H_A(t)]\}/\beta$. Here, the blue and red curves represent the cold ($\beta_2 = 1.0$) isothermal expansion and hot ($\beta_1 = 0.5$) isothermal compression processes, while the purple and orange curves represent the hot isentropic expansion and cold isentropic compression processes, respectively. The cycle starts from the red arrow and evolves in a counterclockwise fashion over time (heat engine). (b) T - S diagram under the same condition as (a).

we have

$$F_A^0(\beta; t) = -\frac{1}{\beta} \ln \left[2 \cosh \left(\beta \sqrt{B^2(t) + E^2} \right) \right]. \quad (27)$$

Then, the conjugate variable $M_A^0(\beta_k; t) \equiv -\partial F_A^0(\beta_k; t)/\partial B$ at the inverse temperature β_k is evaluated as

$$M_A^0(\beta_k; t) = \frac{B(t)}{\sqrt{B^2(t) + E^2}} \tanh \left(\beta_k \sqrt{B^2(t) + E^2} \right). \quad (28)$$

The entropy can also be evaluated by differentiating $F_A^0(\beta; t)$ with respect to β as

$$S_A^0(\beta; t) = k_B \left\{ \ln \left[2 \cosh \left(\beta \sqrt{B^2(t) + E^2} \right) \right] - \beta \sqrt{B^2(t) + E^2} \tanh \left(\beta \sqrt{B^2(t) + E^2} \right) \right\}. \quad (29)$$

This value agrees with von Neumann entropy defined as Eq. (B1), because the subsystem is isolated.

Under the factorized assumption, we can depict the B - M diagram for the isothermal process $B(t)$: (i) $B_1 \rightarrow B_2$ and (iii) $B_3 \rightarrow B_4$ for any form of $B(t)$. To set up isentropic processes (ii) $B_2 \rightarrow B_3$ and (iv) $B_4 \rightarrow B_1$, we have the condition to satisfy (Appendix A)

$$B_b = \sqrt{\frac{\beta_a}{\beta_b} (B_a^2 + E^2) - E^2}, \quad (30)$$

where β_a and β_b are the inverse temperatures of the baths before and after the adiabatic process for $(a, b) = (\text{ii}, \text{iii})$ or (iv, i) , because otherwise entropy is generated. Note that, in the conventional Carnot cycle, the isentropic process is regarded as a temperature-changing process in which the internal energy also changes. In the present

TABLE I. Cycle of the IDF [$B(t)$] and the hot and cold ATFs [$A_1(t)$ and $A_2(t)$] for an eight-stroke Carnot engine. Because we explicitly treat the bath removing and bath attaching processes of hot and cold baths denoted by (i')-(vi'), the cycle consists of the eight strokes. Here, the stroke interval is equally spaced and described as τ . Thus, the cycle period is $T = 8\tau$. The parameters B_1 and B_2 can take any value, while B_3 and B_4 are determined from Eq. (30). We set $B_1 = \sqrt{15}/2$, $B_2 = \sqrt{7}/2$, $B_3 = 1/2$, and $B_4 = \sqrt{3}/2$.

	$B(t)$	$A_1(t)/ A_1 $	$A_2(t)/ A_2 $
(i)	$B_1 + (B_2 - B_1)t/\tau$	1	0
(i')	B_2	$1 - (t - \tau)/\tau$	0
(ii)	$B_2 + (B_3 - B_2)(t - 2\tau)/\tau$	0	0
(ii')	B_3	0	$(t - 3\tau)/\tau$
(iii)	$B_3 + (B_4 - B_3)(t - 4\tau)/\tau$	0	1
(iii')	B_4	0	$1 - (t - 5\tau)/\tau$
(iv)	$B_4 + (B_1 - B_4)(t - 6\tau)/\tau$	0	0
(iv')	B_1	$(t - 7\tau)/\tau$	0

case, we cannot define the temperature during the isentropic process because the system is microscopic and isolated aside from the initial and final states at β_a and β_b . Thus, instead of assuming a spontaneous change in internal energy, here we control the external field (IDF) using Eq. (30) to realize isentropic processes between two different inverse temperatures instead of adiabatic processes.

As in the Carnot cycle, the parameters B_1 and B_2 can have any value, but they must satisfy the relation $B_1 < B_2$ to ensure that the work done by the cycle is positive. In Fig. 1, we depict the B - M diagram for $B_1 = \sqrt{15}/2$ and $B_2 = \sqrt{7}/2$ with $\beta_1/\beta_2 = 2$. In comparison with the P - V diagram for an ideal gas, the rotational direction in the B - M diagram is opposite. This is because an ideal gas is described by $dU = TdS - PdV$, whereas here we have $dU = TdS + BdM$. Thus, this cycle is described as (i) isothermal compression, (ii) isentropic compression, (iii) isothermal expansion, and (iv) isentropic expansion, which is opposite to the P - V case. The area enclosed by the curves corresponds to the work, but a counterclockwise cycle represents positive work, which is also opposite to the P - V case.

B. Cases for non-perturbative and non-Markovian conditions

1. Simulation detail

We now simulate the Carnot engine using our model, which includes not only the IDF but also the ATFs. We will compute $W_{\text{tot}}(t) = W_{A+I}(t)$ for various cycle frequencies Ω . We will then analyze the characteristics of the engine in the quasi-static case using thermodynamic variables defined by the quasi-static free energy $\Delta F_{A+I}^{\text{qst}}(t) = W_{A+I}^{\text{qst}}(t)$. As explained in the factorized case, to realize the isentropic processes, we must change

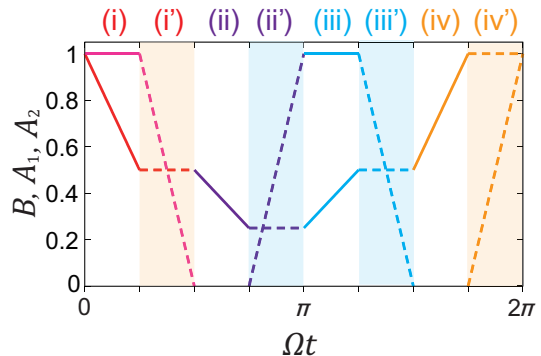


FIG. 2. Time profiles of $B(t)$, $A_1(t)$, and $A_2(t)$ for the eight-stroke Carnot cycle depicted as functions of Ωt , where $\Omega = \pi/4\tau$. The profile of $B(t)$ consists of the red, purple, blue, and orange solid lines corresponding to isothermal and isentropic processes (i)–(iv), and the red, purple, blue, and orange dashed lines corresponding to the bath removing and bath attaching processes of hot and cold baths (i')–(vi'), respectively. The profiles of $A_1(t)$ and $A_2(t)$ consist of the orange dashed, red solid, and red dashed lines, and the purple dashed, blue solid, and blue dashed lines corresponding to the bath attaching, operating, and removing processes (vi'), (i), and (i'), and (ii'), (iii), and (iii'), for the hot and cold baths, respectively.

the IDF after removing or before attaching the heat bath as described by (ii) and (iv). In addition to the regular four Carnot processes (i)–(iv), we must explicitly treat four additional processes that representing (i') removing and (iv') attaching the hot bath and (ii') attaching and (iii') removing the cold bath.

We conduct numerical simulations for the TLS coupled to two bosonic baths at different temperatures using the HEOM approach. Here, we consider the equally spaced stroke period τ . Thus, the cycle period and frequency are $T = 8\tau$ and $\Omega = \pi/4\tau$, respectively. (See Table I and Fig. 2.) Throughout this paper, we fix the system parameters as $E = 0.5$ and the bath parameters as $\beta_1 = 0.5$, $\beta_2 = 1.0$, and $\gamma \equiv \gamma_1 = \gamma_2 = 1.0$ and $A_0 = 0.1, \sqrt{0.1}$, and $\sqrt{3.0}$, where $A_0 \equiv A_1 = A_2$ is the maximum strength of $A_1(t)$ and $A_2(t)$. We chose the truncation number of the hierarchy, representing the depth of the HEOM computation, as $N = 8$ for the $A_0 = \sqrt{3.0}$ case, and $N = 6$ for the other cases. A Padé spectral decomposition scheme was employed to obtain the expansion coefficients of the noise correlation functions.⁹³ We set the number of Padé frequencies as $K_1 = K_2 = 4$. We integrate Eq. (7) from a temporal initial state until the cycle of the simulation reached the steady-state with the time-dependent fields using the fourth-order Runge–Kutta method with a time step of $\delta t = 1.0 \times 10^{-2}$. The various thermodynamic variables can then be evaluated from the HEOM elements.

To reduce the computational time, we set $\hat{\rho}_{\bar{n}}$ to zero for the elements $N_1 > 1$ and $N_2 > 1$ in $\tau \geq 100$, where $N_k = \sum_{l=0}^{K_k} n_l^k$. This treatment is valid because the ADOs of the hot bath are negligibly small by the time the bath is

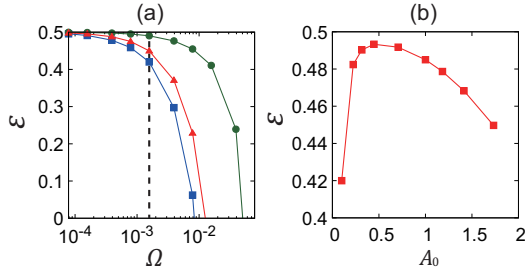


FIG. 3. (a) Efficiencies of the quantum Carnot engine calculated as a function of Ω for different SB coupling strengths: (1) $A_0 = 0.1$ (blue curve with square markers), (2) $A_0 = \sqrt{0.1}$ (green curve with circular markers), and (3) $A_0 = \sqrt{3.0}$ (red curve with triangular markers). (b) Efficiencies of the quantum Carnot cycle as a function of A_0 at the fixed cycle frequency $\Omega/2\pi = 2.5 \times 10^{-4}$, indicated by the dashed line in (a).

restored to the system; the ADOs decay exponentially in time after the baths are removed from the system.

2. Thermal efficiency

We plot the efficiency of the engine, which is significant in the characterization of the Carnot cycle. The total work and heat from the hot bath per cycle W_{tot} and Q_{B_1} are obtained from Eqs. (15)–(17) and Eqs. (12) and (13). The efficiency is then evaluated as

$$\varepsilon = -\frac{W_{\text{tot}}}{Q_{B_1}}. \quad (31)$$

In Fig. 3 (a), we display the efficiency ε as a function of Ω for the weak ($A_0 = 0.1$), intermediate ($A_0 = \sqrt{0.1}$), and strong ($A_0 = \sqrt{3.0}$) SB coupling cases. For any A_0 , the efficiency converges as the Carnot limit $\varepsilon_C = 1 - \beta_H/\beta_C$, which is 0.5 in the present case, for the quasi-static case $\Omega \rightarrow 0$, as the manifestation of the Carnot's theorem.

In Fig. 3 (b), we display the efficiency as a function of the SB-coupling strength A_0 at the fixed cycle frequency $\Omega/2\pi = 2.5 \times 10^{-4}$. When A_0 is small, thermal excitation is weak and the time required for equilibration becomes longer. Conversely, when A_0 is very large, the efficiency decreases. This is because, due to the strong relaxation, the heat bath suppresses the kinetic motion relating to the heat flow.^{48,55,73} Thus, for fixed Ω , the efficiency reaches a maximum in the intermediate region where A_0 is neither large nor small. This feature has been observed in various quantum transport problems, such as exciton transfer⁹⁸ and chemical-reaction problems,⁹⁹ and it is known in the classical case as the Kramers turnover problem. When Ω becomes smaller, the A_0 dependence of the efficiency is suppressed, as can be seen from Fig. 3 (a).

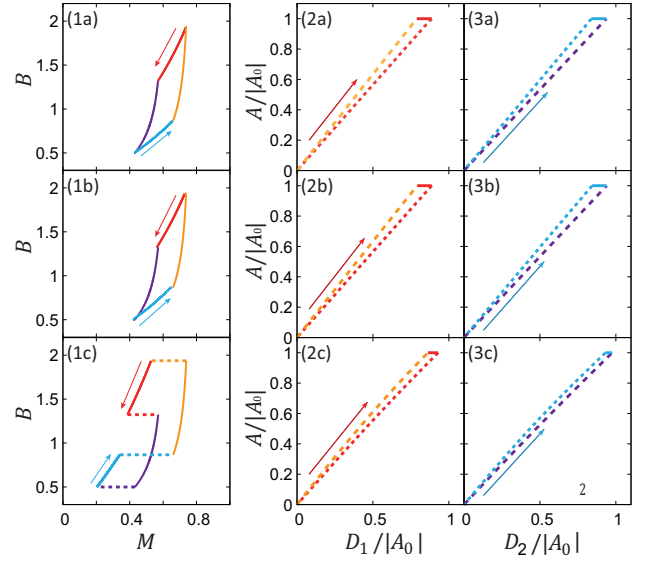


FIG. 4. (1) B - M , (2) A_1 - D_1 , and (3) A_2 - D_2 diagrams for the quasi-static processes with $E = 0.5$ in the weak SB coupling case ($A_0 = 0.1$) (a), in the intermediate SB coupling case ($A_0 = \sqrt{0.1}$) (b), and in the strong SB coupling case ($A_0 = \sqrt{3.0}$) (c). In (1), the B - M diagrams, the red and blue curves represent the (i) hot ($\beta_1 = 0.5$) isothermal compression and (iii) cold ($\beta_2 = 1.0$) isothermal expansion processes, whereas the purple and orange curves represent the (ii) isentropic compression and (iv) isentropic expansion processes, respectively. The cycle starts from the red arrow and evolves in a counterclockwise fashion over time (heat engine). In (2), the A_1 - D_1 diagrams, the red and orange dashed curves represent (i') removing and (iv') attaching the hot bath, whereas, in (3), the A_2 - D_2 diagrams, the purple and blue dashed curves represent (ii') attaching and (iii') removing the cold bath. The cycles in the A_1 - D_1 and A_2 - D_2 diagrams start from the red and blue arrows and evolve in clockwise and counterclockwise fashions over time (refrigerator and heat engine), respectively.

3. B-M and A-D diagrams

Under the quasi-static condition, we can employ a thermodynamic description of the system because the variables defined from the quasi-static free energy by Eqs. (21) and (22) become the state variables.^{73,79,92} By comparing these thermodynamic variables with the physical quantities calculated by HEOM, we can quantitatively verify the qHE description of quantum thermodynamics.

In Fig. 4, we depict the results for the IDF, hot ATF, and cold ATF as the (1) B - M , (2) A_1 - D_1 , and (3) A_2 - D_2 diagrams in the quasi-static case for the (a) weak, (b) intermediate, and (c) strong SB coupling cases. In these diagrams, the bath-removing processes (i') and (iii') and bath-attaching processes (ii') and (iv') are represented as dashed curves. The trajectories of the work diagram are periodical and closed because M , D_1 , and D_2 are the state variables. The area enclosed by each diagram corresponds to negative work when evolving in a coun-

TABLE II. The works done in one cycle for three values of the SB coupling strength A_0 . Here, W_a with $a = B-M$, A_1-D_1 , and A_2-D_2 represents the work evaluated as the areas surrounded by the trajectories of the work diagrams in Fig. ??, and W_b^{HEOM} with $b = B$, A_1 , and A_2 represents the work directly evaluated from the HEOM approach from Eqs. (16) and (17) for the external fields $B(t)$, $A_1(t)$, and $A_2(t)$, respectively. In both cases, the total work is evaluated as $W_{\text{tot}}^{\text{HEOM}} = W_B^{\text{HEOM}} + W_{A_1}^{\text{HEOM}} + W_{A_2}^{\text{HEOM}}$ with $W_{\text{tot}} = W_{\text{tot}}^{\text{HEOM}}$.

A_0	W_{B-M}	W_B^{HEOM}	$W_{A_1-D_1}$	$W_{A_1}^{\text{HEOM}}$	$W_{A_2-D_2}$	$W_{A_2}^{\text{HEOM}}$	$W_{\text{tot}}^{\text{HEOM}}$
0.1	-0.127	-0.127	4.83×10^{-4}	4.83×10^{-4}	-4.90×10^{-4}	-4.90×10^{-4}	-0.127
$\sqrt{0.1}$	-0.128	-0.128	4.81×10^{-3}	4.81×10^{-3}	-4.85×10^{-3}	-4.85×10^{-3}	-0.129
$\sqrt{3.0}$	-0.149	-0.149	0.122	0.122	-0.101	-0.101	-0.128

terclockwise fashion over time, whereas it corresponds to positive work when evolving in a clockwise fashion. We have numerically confirmed that $W_{A+I}(\beta; t)$ evaluated as the areas surrounded by the trajectories of the diagrams and $W_{A+I}^{\text{HEOM}}(t)$ calculated from the HEOM agree. (See table II).

In Figs. 4(2a)-(2c) and 4(3a)-(3c), the positive work done by the hot ATF and the negative work done by the cold ATF are approximately equivalent and almost cancel each other out. Thus, the total work is predominantly determined by the work done by the IDF illustrated in the $B-M$ diagram. In this weak coupling case, the profiles in Fig. 4(1a) thus become similar to that in the factorized assumption case in Fig. 2.

In Fig. 4(1c)-(3c), we present the results for the strong coupling case. The $B-M$ result is quite different from the cases in Figs. 4(1a) and 4(1b) due to the presence of bath removing and bath attaching processes denoted as the dashed lines. If this TLS is regarded as a spin system, $B(t)$ corresponds to the excitation energy of the spin. Then, as $B(t)$ increases, the spin is aligned with the ground state, so the magnetization $M(\beta; t)$ increases. Since the SB interaction with $\hat{V} = \hat{\sigma}_x$ excites the spins, an increase or decrease in $A_k(t)$ causes a decrease or increase in $M(\beta; t)$ even if $B(t)$ is constant.

Similarly, an increase in $B(t)$ suppresses the spin excitation effect of $A_k(t)$, so $D_k(\beta; t)$ decreases even if $A_k(t)$ does not change, as shown by the red and blue horizontal lines in the A_1-D_1 and A_2-D_2 diagrams. Thus, in the strong coupling case in Fig. 4(c), we observe the contribution from the red and orange dashed lines resulting from changes in $A_1(t)$ in processes (i') and (iv') and that from the purple and blue dashed lines resulting from changes in $A_2(t)$ in processes (ii') and (iii'). The areas surrounded by the trajectories of the $B-M$ diagrams are divided vertically into two parts, with the processes evolving in a counterclockwise fashion over time at the top and those evolving in a clockwise fashion over time at the bottom. In this case, the work is evaluated from the area of the top minus the area of the bottom. As we will show using $T-S$ diagram, the bath removing and bath attaching processes determined by ATFs dominate the heat transfer processes in the strong SB interaction case. In Fig. 4(1c), such effects appear as the vertical shifts of the solid curves corresponding to (i)-(iv). Although the profiles of the $B-M$ diagrams are very different when the SB coupling strength is large, the total work done by the external fields is almost same regardless of the SB coupling strength in the quasi-static case, as the manifestation of the Carnot's theorem. (See Table II.) The very weak A_0 dependence seems to indicate that Ω has not yet reached the quasi-static limit.

4. T-S diagram

Next we display the $T-S$ diagram. The change in the quasi-static Boltzmann entropy (qBE) was calculated from Eq.(25) by numerically differentiating $\Delta F_{A+I}^{\text{qst}}(\beta_k; t)$ with respect to β_k for $k = 1$ and 2 using a finite difference method with grid spacing $\Delta\beta = 1.0 \times 10^{-4}$.

Note that, while the $B-M$ and $A-D$ diagrams are useful in interpreting the works that are directly evaluated from the HEOM approach, the situation for the $T-S$ diagram is different because the entropy is purely a thermodynamic variable that is indirectly evaluated through the use of time-independent temperature. Therefore, the $T-S$ diagram is better suited to exploring the thermodynamic features of the system: The area of the $T-S$

diagram is equivalent to the net gain of heat that can be evaluated from the HEOM formalism as the change in the bath energy.

In Fig.5, we depict the $T-S$ diagram for the (a) weak [$A_0 = 0.1$], (b) intermediate [$A_0 = \sqrt{0.1}$], (c) strong [$A_0 = \sqrt{3.0}$] SB interaction cases. After heat-bath is removed, the system is isolated and entropy does not change under the isentropic manipulation described in Sec. III A. For reference, we also plot the results based on the von-Neumann entropy calculated from the zeroth HEOM element as $S_A^{\text{vN}}(t) = -\text{tr}_A\{\hat{\rho}_0(t) \ln \hat{\rho}_0(t)\}$ in Appendix B. The trajectories of the $T-S$ diagram are periodic and closed because the qBE is the state variables. The area enclosed by each diagram corresponds to the positive heat when evolving in a counterclockwise fash-

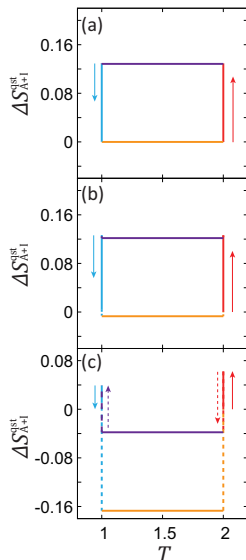


FIG. 5. T - S work diagrams for the quasi-static process ($\Omega/2\pi = 1.25 \times 10^{-5}$) in the (a) weak, (b) intermediate, and (c) strong SB coupling cases corresponding to (a)-(c) in Fig. 4, respectively. The red and blue lines represent the hot and cold isothermal processes, whereas the green and purple dashed-lines are the isentropic compression and expansion process. In each figure, we set $\Delta S_{A+I}^{\text{qst}}(0) = 0$ and the cycle starts from the hot isothermal compression as illustrated by the red arrow. In the strong SB coupling case in (c), the bath removing and bath attaching processes determine the amount of heat production. These processes are represented by the blue and red dashed lines with the dashed arrows that indicate the direction of the cycle.

ion over time. (See table III in Appendix B.)

For the weak and intermediate SB-coupling cases in Fig. 5 (a) and (b), the profiles of the T - S diagram are similar to the factorized case in Fig. 1 (b). This is because the contribution of the entropy from the SB interaction is small in these cases. Conversely, for the strong SB-coupling case in Fig. 5 (c), the T - S diagram differs significantly due to the entropy change associated with the bath removing and bath attaching processes. This is because the system can be excited by the SB interaction through $\hat{V} = \hat{\sigma}_x$, so that entropy increases during the bath attachment process as heat flows from the bath to the system increases, whereas entropy decreases during the bath removing process due to reverse heat flow. Thus, although the area enclosed by the lines that correspond to the net gain of heat is the same as illustrated in Table. III, the heat flow is controlled by the bath attachment and removing processes in the strong coupling case, while the heat flow is controlled by the isothermal process in the weak and intermediate coupling cases. The area enclosed by the trajectory in the T - S diagram corresponds to the net gain of heat and does not depend on the SB coupling strength, as in the case of work.

IV. CONCLUSIONS

We have conducted accurate numerical simulations of a quantum Carnot engine based on a SB model, incorporating the ATFs to describe the effects of adiabatic wall manipulations and the IDF to describe the effects of subsystem manipulation. The HEOM formalism enables the evaluation of the internal energies of not only the subsystem, but also the bath and the SB interactions, even in low-temperature, non-Markovian, and nonperturbative conditions. We analyzed the real-time responses of work as functions of the cycle frequency. As expected, the computational results approach the Carnot efficiency in the quasi-static limit. Moreover, the efficiency does not change regardless of the SB coupling strength, which is also the manifestation of Carnot's theorem.

Moreover, by regarding work as qHE, we compute the conjugate thermodynamic variables of IDF and ATFs to depict the results as thermodynamic work diagrams. We further introduced qBE in an attempt to characterize the thermal properties of the cycle. We showed that work variables such as $M(\beta; t)$ and $D_1(\beta; t)$, and $\Delta S_{A+I}^{\text{qst}}(\beta; t)$ are state variables. Thus the areas surrounded by the trajectories of M - B and D_1 - A_1 diagrams correspond to work, whereas that by the trajectory of T - S diagram corresponds to the net gain of heat. The results show that ATF is responsible for the work when SB coupling is strong and IDF is responsible when it is not. As expected, the total work and net gain of heat were found to be independent of the SB coupling strength in the quasi-static limit, as predicted by Carnot almost 200 years ago. The inclusion of ATF is key to maintain physical consistency in the study of quantum thermodynamics and perhaps quantum information.

Although here we employed a simple spin-boson system, we can apply the same method to ideal gas systems characterized by a P - V diagram by using the hierarchical quantum Fokker-Planck equations.^{32,34} In the case of a Bosonic gas, the results should be similar to those for a classical ideal gas except at very low temperatures; conversely, in the case of a Fermionic gas, the results should exhibit quantum effects even at high temperatures. It would also be interesting to investigate heat engines with different mechanisms, although it seems unlikely that the thermodynamic laws will be violated.

In this investigation, we limited our analysis to work variables in a quasi-static case. As an extension of this study, it is possible to introduce nonequilibrium free energy using the non-equilibrium work. Such investigations are left for future work.

ACKNOWLEDGMENTS

Y.T. was supported by JSPS KAKENHI (Grant No. B21H01884). S.K. acknowledges a fellowship supported by JST, the establishment of university fellowships towards the creation of science technology innovation,

Grant Number JPMJFS2123.

AUTHOR DECLARATIONS

Conflict of Interest

The authors have no conflicts to disclose.

DATA AVAILABILITY

The data that support the findings of this study are available from the corresponding author upon reasonable request.

Appendix A: Isentropic processes

In the classical Carnot cycle, the isentropic process is regarded as a temperature-changing process in which the internal energy also changes. In the present case, we cannot define the temperature during the isentropic process because the system is microscopic and isolated, aside from the initial and final states described by β_1 or β_2 . Thus, instead of assuming a spontaneous change in internal energy, we must adjust the IDF after manipulating the adiabatic wall to realize isentropic processes. Because the heat baths have been removed, we only consider the main system here. For an isentropic process, we have

$$dU_A = -M_A^0 dB, \quad (\text{A1})$$

because the change in entropy is zero. Alternatively, the internal energy is expressed as

$$dU_A = \left(\frac{\partial U_A}{\partial \beta} \right)_B d\beta + \left(\frac{\partial U_A}{\partial B} \right)_\beta dB. \quad (\text{A2})$$

Because the internal energy of the TLS is evaluated from Eq. (27) as

$$U_A^0(t) = -\sqrt{B^2(t) + E^2} \tanh(\beta \sqrt{B^2(t) + E^2}), \quad (\text{A3})$$

we have

$$\left(\frac{\partial U_A}{\partial \beta} \right)_B = -\frac{B^2(t) + E^2}{\cosh^2(\beta \sqrt{B^2(t) + E^2})}, \quad (\text{A4})$$

$$\left(\frac{\partial U_A}{\partial B} \right)_\beta = -\frac{B(t)}{\sqrt{B^2(t) + E^2}} \tanh(\beta \sqrt{B^2(t) + E^2}) - \frac{\beta B(t)}{\cosh^2(\beta \sqrt{B^2(t) + E^2})}. \quad (\text{A5})$$

From Eqs. (A1) and (A2), we have the relation

$$-(B^2 + E^2)d\beta = \beta B dB. \quad (\text{A6})$$

TABLE III. The net gain of heat evaluated as the area in the T - S diagrams based on the quasi-static Boltzmann entropy [Q_{qBE}] and von Neumann entropy [Q_{vNE}] for different SB coupling strength A_0 . They are compared with the one cycle of bath energy [$Q_{tot}^{\text{HEOM}} \equiv \Delta U_{B_1}^{\text{qst}}(\beta_1; t) + \Delta U_{B_2}^{\text{qst}}(\beta_2; t)$] evaluated using Eq.(13) from the HEOM approach.

A_0	Q_{qBE}	Q_{vNE}	Q_{tot}^{HEOM}
0.1	0.1285	0.1289	0.1272
$\sqrt{0.1}$	0.1286	0.1289	0.1287
$\sqrt{3.0}$	0.1292	0.1290	0.1283

For isentropic processes from $B(t_a) = B_a$ at β_a to $B(t_b) = B_b$ at β_B , we have

$$-\ln\left(\frac{\beta_b}{\beta_a}\right) = \ln\left(\frac{\sqrt{E^2 + B_b^2}}{\sqrt{E^2 + B_a^2}}\right). \quad (\text{A7})$$

Thus, we have the relation

$$B_b = \sqrt{\frac{\beta_a}{\beta_b} (B_a^2 + E^2) - E^2}. \quad (\text{A8})$$

Appendix B: Quasi-static Boltzmann entropy and von Neumann entropy

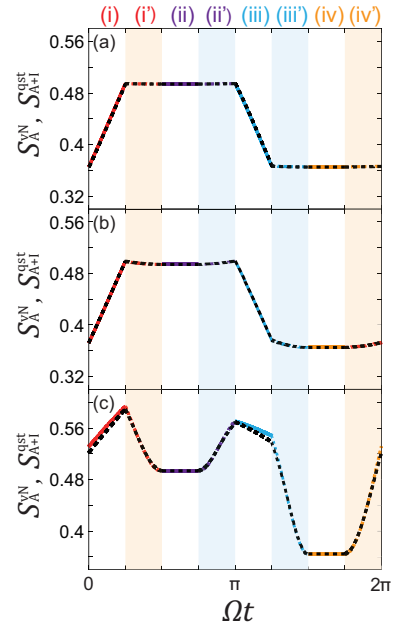


FIG. 6. The time evolution of the qBE (color curves) and von-Neumann entropy (black dashed-curves) in the (a) weak, (b) intermediate, and (c) strong SB-coupling cases for eight-stroke cycle denoted by (i)-(iv'). (For the correspondence between each stroke and the color of the line, see Fig. 2.)

The von Neumann entropy is commonly used in quantum thermodynamics, in particular in non-equilibrium

cases. It is defined as the following:

$$S_A^{\text{vNE}}(t) = -\text{tr}_A\{\hat{\rho}_A(t) \ln \hat{\rho}_A(t)\}, \quad (\text{B1})$$

where $\hat{\rho}_A(t)$ is the reduced density matrix. In isolated systems, both quasi-static Boltzmann entropy (qBE) and von Neumann entropy (vNE) are equivalent, but in a reduced system, this equivalence does not hold due to the contribution of entropy from the SB interaction. Then, it was found that if we use the reduced density matrix obtained from non-perturbative approaches, such as the HEOM approach, the description of vNE becomes reasonably accurate even in the strong SB coupling case.⁷³ Here, using the zeroth member of the HEOM solution in Eq. (B1) as $\hat{\rho}_A(t) = \hat{\rho}_0$, we introduce the vNE to characterize the time evolution of qBE more closely. Because the Carnot cycle involves two isentropic processes, where the qBE and vNE results must agree, we can verify the description of vNE in the isotropic processes, as well as the transitions between the isentropic and isothermal processes.

Using the calculated entropy, we also computed the net gain of heat per cycle. For example, for the vNE, Q_{vNE} is evaluated as

$$Q_{\text{vNE}} = \int_{-\frac{\pi}{4\Omega}}^{\frac{\pi}{2\Omega}} dt T_1 \frac{\partial S_A^{\text{vNE}}(\beta_1; t)}{\partial t} + \int_{\frac{3\pi}{4\Omega}}^{\frac{3\pi}{2\Omega}} dt T_2 \frac{\partial S_A^{\text{vNE}}(\beta_2; t)}{\partial t}. \quad (\text{B2})$$

Calculated results are presented in Table III. While the net gain of heat calculated directly in HEOM agrees with the total work presented in Table II, there is a slight discrepancy between $Q_{\text{tot}}^{\text{HEOM}}$ and the other values obtained from qBE and vNE. This may be due to the insufficient precision of the β derivative to evaluate entropy.

In Fig. 6, we depict the qBE and vNE as a function of time for different SB coupling strength. Here, we adjust $S_{A+1}^{\text{qst}}(t) = S_A^{\text{vNE}}(t)$ at $t = \pi/2\Omega$. As illustrated in Fig. 6(a) and 6(b), the results from the qBE and vNE are similar and almost overlapped. This is because the contribution of the entropy from the SB interaction is small in these cases. In the strong coupling case in (c), while the time evolution of entropy in isentropic processes is similar, that in isothermal processes controlled by $B(t)$ are different. This is because the contribution of the entropy from the SB interaction is not considered in the vNE due to its reduced description of the system. Thus, the vNE underestimates the entropy compared with qBE in the isothermal processes. Because their contribution cancels out, the net gain of heat evaluated as the area in T - S diagrams is similar in both qBE and vNE cases, as presented in Table III.

¹S. Carnot, *Reflexions sur la puissance motrice du feu* (Chez Bachelier Libraire, Quai des Augustins, Paris, 1824).

²B. P. E. Clapeyron, "Memoire sur la puissance motrice de la chaleur," *Journal de l' Ecole Royale Polytechnique* **14**, 153–190 (1834).

³W. Thomson, "On an absolute thermometric scale founded on carnot's theory of the motive power of heat," *Cambridge Philosophical Society Proceedings for June 5; and Phil. Mag.*, Oct. , 100–106 (1848).

⁴R. Clausius, "Ueber die bewegende kraft der wärme und die gesetze, welche sich daraus für die wärmelehre selbst ableiten lassen," *Annalen der Physik* **155**, 500–524 (1850).

⁵R. Clausius, "Ueber die anwendung der mechanischen wärmetheorie auf die dampfmaschine," *Annalen der Physik* **173**, 513–558 (1856).

⁶R. Clausius, "Ueber verschiedene für die anwendung bequeme formen der hauptgleichungen der mechanischen wärmetheorie," *Annalen der Physik* **201**, 353–400 (1865).

⁷F. Binder, L. A. Correa, G. C. J. Anders, and G. A. (Eds.), *Thermodynamics in the Quantum Regime* (Springer International Publishing, 2018).

⁸R. Kosloff, "Quantum thermodynamics: A dynamical viewpoint," *Entropy* **15**, 2100–2128 (2013).

⁹R. Härtle, G. Cohen, D. R. Reichman, and A. J. Millis, "Decoherence and lead-induced interdot coupling in nonequilibrium electron transport through interacting quantum dots: A hierarchical quantum master equation approach," *Phys. Rev. B* **88**, 235426 (2013).

¹⁰M. F. Ludovico, J. S. Lim, M. Moskalets, L. Arrachea, and D. Sánchez, "Dynamical energy transfer in ac-driven quantum systems," *Phys. Rev. B* **89**, 161306 (2014).

¹¹M. Esposito, M. A. Ochoa, and M. Galperin, "Quantum thermodynamics: A nonequilibrium green's function approach," *Phys. Rev. Lett.* **114**, 080602 (2015).

¹²G. Cohen and M. Galperin, "Green's function methods for single molecule junctions," *The Journal of Chemical Physics* **152**, 090901 (2020), <https://doi.org/10.1063/1.5145210>.

¹³F. Brandão, M. Horodecki, N. Ng, J. Oppenheim, and S. Wehner, "The second laws of quantum thermodynamics," *112*, 3275–3279 (2015).

¹⁴P. Haughian, M. Esposito, and T. L. Schmidt, "Quantum thermodynamics of the resonant-level model with driven system-bath coupling," *Phys. Rev. B* **97**, 085435 (2018).

¹⁵M. Perarnau-Llobet, H. Wilming, A. Riera, R. Gallego, and J. Eisert, "Strong coupling corrections in quantum thermodynamics," *Phys. Rev. Lett.* **120**, 120602 (2018).

¹⁶K. Funo and H. T. Quan, "Path integral approach to heat in quantum thermodynamics," *Phys. Rev. E* **98**, 012113 (2018).

¹⁷A. Rivas, "Strong coupling thermodynamics of open quantum systems," *Phys. Rev. Lett.* **124**, 160601 (2020).

¹⁸L. M. Cangemi, V. Cataudella, G. Benenti, M. Sassetti, and G. De Filippis, "Violation of thermodynamics uncertainty relations in a periodically driven work-to-work converter from weak to strong dissipation," *Phys. Rev. B* **102**, 165418 (2020).

¹⁹P. Talkner and P. Hänggi, "Colloquium: Statistical mechanics and thermodynamics at strong coupling: Quantum and classical," *Rev. Mod. Phys.* **92**, 041002 (2020).

²⁰S. An, J.-N. Zhang, M. Um, D. Lv, Y. Lu, J. Zhang, Z.-Q. Yin, H. T. Quan, and K. Kim, "Experimental test of the quantum jarzynski equality with a trapped-ion system," *Nature Physics* **11**, 193 (2015).

²¹S. An, D. Lv, del Campo Adolfo, and K. Kim, "Shortcuts to adiabaticity by counterdiabatic driving for trapped-ion displacement in phase space," *Nature Communications* **7**, 12999 (2016).

²²N. V. Vitanov, A. A. Rangelov, B. W. Shore, and K. Bergmann, "Stimulated raman adiabatic passage in physics, chemistry, and beyond," *Rev. Mod. Phys.* **89**, 015006 (2017).

²³E. A. Hoffmann, S. Fahlvik, C. Thelander, M. Leijnse, and H. Linke, "A quantum-dot heat engine operating close to the thermodynamic efficiency limits," *Nature Nanotechnology* **13**, 920–924 (2018).

²⁴J. Bengtsson, M. N. Tengstrand, A. Wacker, P. Samuelsson, M. Ueda, H. Linke, and S. M. Reimann, "Quantum szilard engine with attractively interacting bosons," *Phys. Rev. Lett.* **120**, 100601 (2018).

²⁵M. Josefsson, A. Svilans, H. Linke, and M. Leijnse, "Optimal power and efficiency of single quantum dot heat engines: Theory and experiment," *Phys. Rev. B* **99**, 235432 (2019).

- ²⁶D. Prete, P. A. Erdman, V. Demontis, V. Zannier, D. Ercolani, L. Sorba, F. Beltram, F. Rossella, F. Taddei, and S. Roddaro, “Thermoelectric conversion at 30 k in inas/inp nanowire quantum dots,” *Nano Letters* **19**, 3033–3039 (2019), pMID: 30935206.
- ²⁷Y.-H. Ma, R.-X. Zhai, J. Chen, C. P. Sun, and H. Dong, “Experimental test of the $1/\tau$ -scaling entropy generation in finite-time thermodynamics,” *Phys. Rev. Lett.* **125**, 210601 (2020).
- ²⁸A. de Oliveira, R. Gomes, V. Brasil, N. Rubiano da Silva, L. Céleri, and P. Souto Ribeiro, “Full thermalization of a photonic qubit,” *Physics Letters A* **384**, 126933 (2020).
- ²⁹S. Hernández-Gómez, N. Staudenmaier, M. Campisi, and N. Fabbri, “Experimental test of fluctuation relations for driven open quantum systems with an NV center,” *New Journal of Physics* **23**, 065004 (2021).
- ³⁰S. Ryu, R. López, L. Serra, and D. Sánchez, “Beating carnot efficiency with periodically driven chiral conductors,” *Nature Communications* **13**, 2512 (2022).
- ³¹Y. Tanimura, “Stochastic liouville, langevin, fokker-planck, and master equation approaches to quantum dissipative systems,” *Journal of the Physical Society of Japan* **75**, 082001 (2006).
- ³²Y. Tanimura, “Numerically ”exact” approach to open quantum dynamics: The hierarchical equations of motion (heom),” *The Journal of Chemical Physics* **153**, 020901 (2020).
- ³³Y. Tanimura, “Reduced hierarchical equations of motion in real and imaginary time: Correlated initial states and thermodynamic quantities,” *The Journal of Chemical Physics* **141**, 044114 (2014).
- ³⁴Y. Tanimura, “Real-time and imaginary-time quantum hierarchal fokker-planck equations,” *The Journal of Chemical Physics* **142**, 144110 (2015).
- ³⁵D. Segal, A. Nitzan, and P. Hänggi, “Thermal conductance through molecular wires,” *The Journal of Chemical Physics* **119**, 6840–6855 (2003), <https://doi.org/10.1063/1.1603211>.
- ³⁶D. Segal and A. Nitzan, “Spin-boson thermal rectifier,” *Phys. Rev. Lett.* **94**, 034301 (2005).
- ³⁷D. Segal, “Heat flow in nonlinear molecular junctions: Master equation analysis,” *Phys. Rev. B* **73**, 205415 (2006).
- ³⁸N. Boudjada and D. Segal, “From dissipative dynamics to studies of heat transfer at the nanoscale: Analysis of the spin-boson model,” *The Journal of Physical Chemistry A* **118**, 11323–11336 (2014), pMID: 25396751.
- ³⁹A. Dhar, “Heat transport in low-dimensional systems,” *Advances in Physics* **57**, 457–537 (2008).
- ⁴⁰K. A. Velizhanin, H. Wang, and M. Thoss, “Heat transport through model molecular junctions: A multilayer multiconfiguration time-dependent hartree approach,” *Chemical Physics Letters* **460**, 325–330 (2008).
- ⁴¹Y. Dubi and M. Di Ventra, “Colloquium: Heat flow and thermoelectricity in atomic and molecular junctions,” *Rev. Mod. Phys.* **83**, 131–155 (2011).
- ⁴²C. Wang, J. Ren, and J. Cao, “Nonequilibrium energy transfer at nanoscale: A unified theory from weak to strong coupling,” *Scientific Reports* **5** (2015), 10.1038/srep11787.
- ⁴³K. Saito and T. Kato, “Kondo signature in heat transfer via a local two-state system,” *Phys. Rev. Lett.* **111**, 214301 (2013).
- ⁴⁴L. Song and Q. Shi, “Hierarchical equations of motion method applied to nonequilibrium heat transport in model molecular junctions: Transient heat current and high-order moments of the current operator,” *Phys. Rev. B* **95**, 064308 (2017).
- ⁴⁵E. Aurell and F. Montana, “Thermal power of heat flow through a qubit,” *Phys. Rev. E* **99**, 042130 (2019).
- ⁴⁶M. Kilgour, B. K. Agarwalla, and D. Segal, “Path-integral methodology and simulations of quantum thermal transport: Full counting statistics approach,” *The Journal of Chemical Physics* **150**, 084111 (2019).
- ⁴⁷M. Xu, J. T. Stockburger, and J. Ankerhold, “Heat transport through a superconducting artificial atom,” *Phys. Rev. B* **103**, 104304 (2021).
- ⁴⁸A. Kato and Y. Tanimura, “Quantum heat transport of a two-qubit system: Interplay between system-bath coherence and qubit-qubit coherence,” *The Journal of Chemical Physics* **143**, 064107 (2015).
- ⁴⁹M. Esposito, M. A. Ochoa, and M. Galperin, “Nature of heat in strongly coupled open quantum systems,” *Phys. Rev. B* **92**, 235440 (2015).
- ⁵⁰H. T. Quan, Y.-x. Liu, C. P. Sun, and F. Nori, “Quantum thermodynamic cycles and quantum heat engines,” *Phys. Rev. E* **76**, 031105 (2007).
- ⁵¹N. Brunner, M. Huber, N. Linden, S. Popescu, R. Silva, and P. Skrzypczyk, “Entanglement enhances cooling in microscopic quantum refrigerators,” *Phys. Rev. E* **89**, 032115 (2014).
- ⁵²L. Chotorlishvili, Z. Toklikishvili, and J. Berakdar, “Thermal entanglement and efficiency of the quantum otto cycle for the su(1,1) tavis–cummings system,” **44**, 165303 (2011).
- ⁵³R. Kosloff and A. Levy, “Quantum heat engines and refrigerators: Continuous devices,” *Annual Review of Physical Chemistry* **65**, 365–393 (2014), pMID: 24689798.
- ⁵⁴R. Uzdin, A. Levy, and R. Kosloff, “Equivalence of quantum heat machines, and quantum-thermodynamic signatures,” *Phys. Rev. X* **5**, 031044 (2015).
- ⁵⁵A. Kato and Y. Tanimura, “Quantum heat current under non-perturbative and non-markovian conditions: Applications to heat machines,” *The Journal of Chemical Physics* **145**, 224105 (2016).
- ⁵⁶Y. Y. Xu, B. Chen, and J. Liu, “Achieving the classical carnot efficiency in a strongly coupled quantum heat engine,” *Phys. Rev. E* **97**, 022130 (2018).
- ⁵⁷S. Restrepo, J. Cerrillo, P. Strasberg, and G. Schaller, “From quantum heat engines to laser cooling: Floquet theory beyond the born–markov approximation,” **20**, 053063 (2018).
- ⁵⁸M. Kilgour and D. Segal, “Coherence and decoherence in quantum absorption refrigerators,” *Phys. Rev. E* **98**, 012117 (2018).
- ⁵⁹A. Das and V. Mukherjee, “Quantum-enhanced finite-time otto cycle,” *Physical Review Research* **2** (2020), 10.1103/physrevresearch.2.033083.
- ⁶⁰P. A. Camati, J. F. G. Santos, and R. M. Serra, “Employing non-markovian effects to improve the performance of a quantum otto refrigerator,” *Phys. Rev. A* **102**, 012217 (2020).
- ⁶¹R. S. Johal and V. Mehta, “Quantum heat engines with complex working media, complete otto cycles and heuristics,” *Entropy* **23** (2021), 10.3390/e23091149.
- ⁶²K. Ono, S. N. Shevchenko, T. Mori, S. Moriyama, and F. Nori, “Analog of a quantum heat engine using a single-spin qubit,” *Phys. Rev. Lett.* **125**, 166802 (2020).
- ⁶³M. Wiedmann, J. T. Stockburger, and J. Ankerhold, “Non-markovian dynamics of a quantum heat engine: out-of-equilibrium operation and thermal coupling control,” *New Journal of Physics* **22**, 033007 (2020).
- ⁶⁴M. Wiedmann, J. T. Stockburger, and J. Ankerhold, “Non-markovian quantum otto refrigerator,” *Eur. Phys. J. Spec. Tops* **230**, 851–857 (2021).
- ⁶⁵M. Xu, J. T. Stockburger, G. Kurizki, and J. Ankerhold, “Minimal quantum thermal machine in a bandgap environment: non-markovian features and anti-zeno advantage,” *New Journal of Physics* **24**, 035003 (2022).
- ⁶⁶M. Brenes, J. J. Mendoza-Arenas, A. Purkayastha, M. T. Mitchison, S. R. Clark, and J. Goold, “Tensor-network method to simulate strongly interacting quantum thermal machines,” *Phys. Rev. X* **10**, 031040 (2020).
- ⁶⁷N. Pancotti, M. Scandi, M. T. Mitchison, and M. Perarnau-Llobet, “Speed-ups to isothermality: Enhanced quantum thermal machines through control of the system-bath coupling,” *Phys. Rev. X* **10**, 031015 (2020).
- ⁶⁸S. Lee, M. Ha, J.-M. Park, and H. Jeong, “Finite-time quantum otto engine: Surpassing the quasistatic efficiency due to friction,” *Phys. Rev. E* **101**, 022127 (2020).

- ⁶⁹S. H. Raja, S. Maniscalco, G. S. Paraoanu, J. P. Pekola, and N. L. Gullo, “Finite-time quantum stirling heat engine,” *New Journal of Physics* **23**, 033034 (2021).
- ⁷⁰F. Ivander, N. Anto-Sztrikacs, and D. Segal, “Strong system-bath coupling effects in quantum absorption refrigerators,” *Phys. Rev. E* **105**, 034112 (2022).
- ⁷¹K. Goyal, X. He, and R. Kawai, “Entropy production of a small quantum system under strong coupling with an environment: A computational experiment,” *Physica A: Statistical Mechanics and its Applications* **552**, 122627 (2020).
- ⁷²N. Seshadri and M. Galperin, “Entropy and information flow in quantum systems strongly coupled to baths,” *Phys. Rev. B* **103**, 085415 (2021).
- ⁷³S. Sakamoto and Y. Tanimura, “Numerically ”exact” simulations of entropy production in the fully quantum regime: Boltzmann entropy vs von neumann entropy,” *The Journal of Chemical Physics* **153**, 234107 (2020).
- ⁷⁴R. Schmidt, M. F. Carusela, J. P. Pekola, S. Suomela, and J. Ankerhold, “Work and heat for two-level systems in dissipative environments: Strong driving and non-markovian dynamics,” *Phys. Rev. B* **91**, 224303 (2015).
- ⁷⁵J. Goold, M. Huber, A. Riera, L. del Rio, and P. Skrzypczyk, “The role of quantum information in thermodynamics—a topical review,” **49**, 143001 (2016).
- ⁷⁶P. Strasberg, G. Schaller, T. Brandes, and M. Esposito, “Quantum and information thermodynamics: A unifying framework based on repeated interactions,” *Phys. Rev. X* **7**, 021003 (2017).
- ⁷⁷C. Jarzynski, “Nonequilibrium work theorem for a system strongly coupled to a thermal environment,” *Journal of Statistical Mechanics: Theory and Experiment* **2004**, P09994 (2004).
- ⁷⁸S. Yukawa, “A quantum analogue of the jarzynski equality,” *Journal of the Physical Society of Japan* **69**, 2367–2370 (2000).
- ⁷⁹S. Sakamoto and Y. Tanimura, “Open quantum dynamics theory for non-equilibrium work: Hierarchical equations of motion approach,” *Journal of the Physical Society of Japan* **90**, 033001 (2021).
- ⁸⁰M. Campisi, P. Talkner, and P. Hänggi, “Fluctuation theorem for arbitrary open quantum systems,” *Phys. Rev. Lett.* **102**, 210401 (2009).
- ⁸¹M. Esposito, U. Harbola, and S. Mukamel, “Nonequilibrium fluctuations, fluctuation theorems, and counting statistics in quantum systems,” *Rev. Mod. Phys.* **81**, 1665–1702 (2009).
- ⁸²U. Seifert, “Stochastic thermodynamics, fluctuation theorems and molecular machines,” **75**, 126001 (2012).
- ⁸³M. Campisi, P. Hänggi, and P. Talkner, “Colloquium: Quantum fluctuation relations: Foundations and applications,” *Rev. Mod. Phys.* **83**, 771–791 (2011).
- ⁸⁴E. Aurell, B. Donvil, and K. Mallick, “Large deviations and fluctuation theorem for the quantum heat current in the spin-boson model,” *Phys. Rev. E* **101**, 052116 (2020).
- ⁸⁵R. S. Whitney, “Non-markovian quantum thermodynamics: Laws and fluctuation theorems,” *Phys. Rev. B* **98**, 085415 (2018).
- ⁸⁶H. T. Quan, Y. D. Wang, Y.-x. Liu, C. P. Sun, and F. Nori, “Maxwell’s demon assisted thermodynamic cycle in superconducting quantum circuits,” *Phys. Rev. Lett.* **97**, 180402 (2006).
- ⁸⁷K. Maruyama, F. Nori, and V. Vedral, “Colloquium: The physics of maxwell’s demon and information,” *Rev. Mod. Phys.* **81**, 1–23 (2009).
- ⁸⁸H. Leff and A. F. Rex, “Maxwell’s demon 2 entropy, classical and quantum information, computing,” (2002).
- ⁸⁹Y. Tanimura and R. Kubo, “Time evolution of a quantum system in contact with a nearly gaussian-markoffian noise bath,” *Journal of the Physical Society of Japan* **58**, 101–114 (1989).
- ⁹⁰Y. Tanimura, “Nonperturbative expansion method for a quantum system coupled to a harmonic-oscillator bath,” *Phys. Rev. A* **41**, 6676–6687 (1990).
- ⁹¹A. Ishizaki and Y. Tanimura, “Quantum dynamics of system strongly coupled to low-temperature colored noise bath: Reduced hierarchy equations approach,” *Journal of the Physical Society of Japan* **74**, 3131–3134 (2005).
- ⁹²S. Koyanagi and Y. Tanimura, “The laws of thermodynamics for quantum dissipative systems: A quasi-equilibrium helmholtz energy approach,” *The Journal of Chemical Physics* **157**, 014104 (2022), <https://doi.org/10.1063/5.0093666>.
- ⁹³J. Hu, R.-X. Xu, and Y. Yan, “Communication: Padé spectrum decomposition of fermi function and bose function,” *The Journal of Chemical Physics* **133**, 101106 (2010).
- ⁹⁴A. Lenard, “Thermodynamical proof of the gibbs formula for elementary quantum systems,” *Journal of Statistical Physics* **19**, 575 (1978).
- ⁹⁵H. Tasaki, “Jarzynski relations for quantum systems and some applications,” (2000), [arXiv:cond-mat/0009244 \[cond-mat.stat-mech\]](https://arxiv.org/abs/cond-mat/0009244).
- ⁹⁶Y. Oono, *Perspectives on Statistical Thermodynamics* (Cambridge University Press, 2017).
- ⁹⁷J. Zhang and Y. Tanimura, “Imaginary-time hierarchical equations of motion for thermodynamic variables,” *The Journal of Chemical Physics* **156**, 174112 (2022).
- ⁹⁸A. Ishizaki and G. R. Fleming, “On the adequacy of the redfield equation and related approaches to the study of quantum dynamics in electronic energy transfer,” *The Journal of Chemical Physics* **130**, 234110 (2009).
- ⁹⁹Y. Tanimura and P. G. Wolynes, “The interplay of tunneling, resonance, and dissipation in quantum barrier crossing: A numerical study,” *The Journal of Chemical Physics* **96**, 8485–8496 (1992).